Journal of Nuclear Materials 385 (2009) 231–235

Contents lists available at ScienceDirect

Journal of Nuclear Materials

journal homepage: www.elsevier.com/locate/jnucmat

High-resolution transmission electron microscopy and electron backscatter diffraction in nanoscaled ferritic and ferritic–martensitic oxide dispersion strengthened–steels

Ch.Ch. Eiselt [a,*], M. Klimenkov [a], R. Lindau [a], A. Möslang [a], H.R.Z. Sandim [b], A.F. Padilha [c], D. Raabe [d]

[a] Forschungszentrum Karlsruhe/IMF I, P.O. Box 3640, 72061 Karlsruhe, Germany
[b] Department of Materials Engineering, EEL, University of São Paulo, 12600-970 Lorena, Brazil
[c] Department of Metallurgical and Materials Engineering, Escola Politécnica, University of São Paulo, 05508-900 São Paulo, Brazil
[d] Max-Planck-Institut für Eisenforschung, Max-Planck Strasse 1, D-40237 Düsseldorf, Germany

ARTICLE INFO

PACS:
28.52.Fa
61.46.–w

ABSTRACT

For specific blanket and divertor applications in future fusion power reactors a replacement of presently considered reduced activation ferritic martensitic (RAFM) steels as a structural material by suitable oxide dispersion strengthened ferritic martensitic steels would allow a substantial increase of the operating temperature from ~823 to about 923 K. Due to this reason the RAFM-alloy ODS-Eurofer has already been developed and produced with industrial partners. In the He-cooled modular divertor concept, where temperatures above 923 K will arise, an ODS-steel with a purely ferritic matrix is advantageous, because of missing phase transitions. Due to this reason, a special ferritic ODS-steel is being manufactured as well. In this work the microstructures of these two ODS-alloy types, analysed mainly by high resolution TEM are compared, with respect to different manufacturing processes. In addition first results of high resolution EBSD scans together with determined orientation maps of the RAFM steel ODS-Eurofer will also be presented.

1. Introduction

Fusion power plants shall be part of a future global environmental friendly energy scenario. To achieve this challenging aim, it is very important that suitable structural materials for such kinds of plants are provided. They need to withstand all upcoming loads, high surface heat fluxes, neutron radiation damages, integral dose rates and different reactor operation modes. Due to this situation, these materials must equally cope with complex coolant influences and high temperature creep deformations for many years.

The initial point was the development of the so-called reduced activated ferritic martensitic steels (RAFM), like the Eurofer alloy, which could be applied to a maximum temperature of 823 K. In order to increase the overall efficiency of advanced fusion (DEMO and beyond) or fission power plants (Gen. 4), a general process temperature raise is required. To meet this aim the international development has concentrated on special high temperature performance materials. Generally reduced activated ferritic and martensitic steels (RAFM) as well as reduced activated ferritic steels (RAF), both strengthened through nanoscaled, oxidic dispersoids, serve as a basis for such newly designed alloys. A first generation of oxide dispersion strengthened (ODS)-alloys, called ODS-Eurofer, has already been developed and produced in cooperation with industrial partners [1]. After long-time creep analyses with fusion relevant temperature and stress levels, an increase of the upper operational temperature from 823 to 923 K, as well as improvements in ductility and fracture toughness, could be achieved. Due to higher temperatures (<973 K) in the He-cooled modular divertor concept, the use of RAF-ODS-steels, which are not limited by a phase transition, is required. Therefore, based on the promising results with ODS-Eurofer, a second generation of high performance ferritic ODS-materials is currently being developed [2,3].

2. Experimental

Generally the powder metallurgical route has been applied to manufacture both high performance ODS-material types, including the production steps mechanical alloying, hot isostatic pressing and thermo-mechanical treatments.

The RAFM ODS-Eurofer (9Cr–1W–0.3Y_2O_3) alloy has been produced in cooperation with Plansee AG (Austria). The initial RAFM steel powder together with the oxidic additives was mechanically alloyed in industrial ball mills, with definite milling parameters. After hot isostatic pressing at Plansee AG, ODS-Eurofer bars and rods with special dimensions were fabricated and from these parts

* Corresponding author.
E-mail address: charles.eiselt@imf.fsk.de (Ch.Ch. Eiselt).

0022-3115/$ - see front matter © 2008 Elsevier B.V. All rights reserved.
doi:10.1016/j.jnucmat.2008.11.029

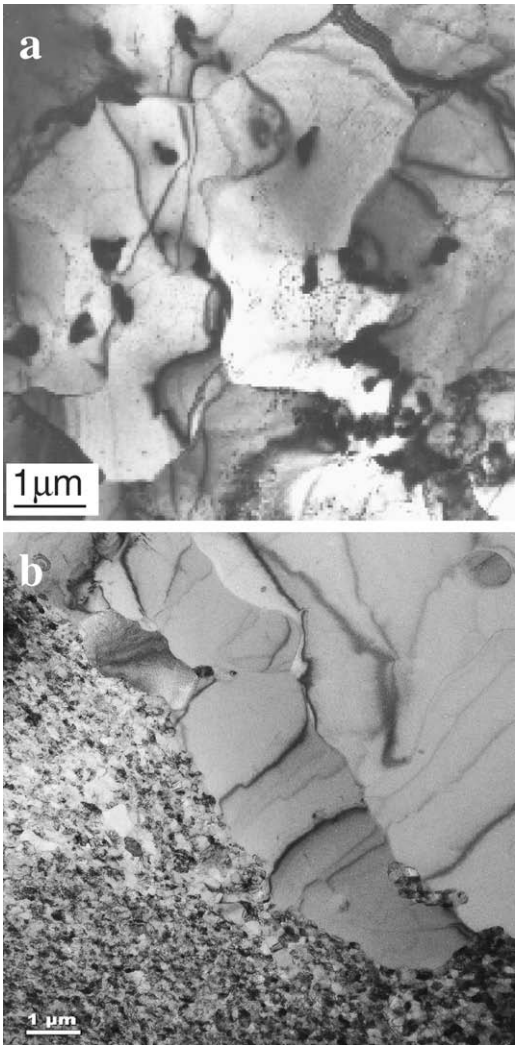

Fig. 1. BFTEM images of (a) RAFM-ODS-Eurofer (9Cr–1W–0.3Y_2O_3) and (b) RAF-ODS-alloy (13Cr–1W–0.3Y_2O_3).

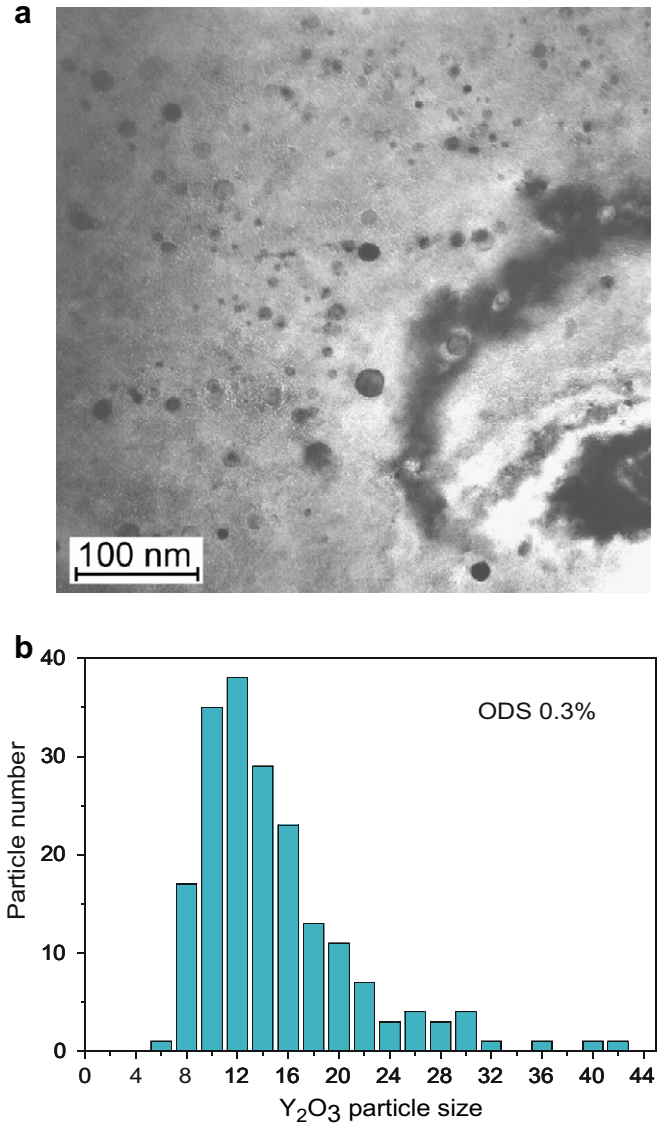

Fig. 2. (a) BFTEM image of RAFM ODS-Eurofer (9Cr–1W–0.3Y_2O_3) and (b) average Y_2O_3 particle size distribution (size step 2 nm).

samples for transmission electron microscopic (TEM) analyses were prepared.

The RAF-ODS-alloy was designed, keeping the following composition: 13Cr–1W–0.3Ti–0.3Y_2O_3. Similarly the basic powders were ball milled in a ZOZ Attritor Simoloyer CM01 with alternating milling parameters such as milling time or milling speed. After predensification and degassing, the alloyed powders were also hot isostatically pressed to full density using special HIP-parameters.

Following, TEM samples could be obtained from this material, applying electropolishing and precise ion polishing according to a definite preparation route [2]. All TEM investigations were performed in Philips CM30 (300 kV) and FEI TECNAI-20F microscopes.

Slabs of the ODS-Eurofer steel were cold rolled to 50% and 80% reductions in multiple passes. Annealing was carried in vacuum at 1073 K for 1 h. High-resolution EBSD mappings with a step size of 50 nm were performed in the longitudinal section of both samples in order to investigate the recrystallization behavior. The microstructure of the annealed specimens was imaged using a JEOL-6500F field emission gun scanning electron microscope (FEG-SEM) operating at 15 kV. Mesotexture data were conducted by automated acquisition and further indexing of Kikuchi patterns after image processing in a TSL system interfaced to the SEM. Vickers microhardness testing was performed in the longitudinal section of the specimens using a load of 200 g.

3. Results

3.1. Microstructural analyses

Fig. 1(a) and (b) displays bright field TEM images confronting the microstructures of both ODS-alloy types. It can be seen that the RAFM-ODS-Eurofer alloy exhibits equiaxed grains with a size of 2–8 µm. This structure is quite homogeneous and exists in all analysed samples. On the contrary, the ferritic ODS-alloy (Fig. 1(b)) has two clearly visible regions with distinct grain size distributions: in one area there are grain sizes of 1–8 µm, similarly to ODS-Eurofer. The other one consists of roundly shaped nanometer-sized grains with dimensions of about 20–500 nm. This phenomenon was identified as a bimodal grain size distribution [2,4–6]. In Ref. [2] it was also shown, that there exists a certain dependency between the applied milling parameters and the extension of the nanograin phase. For ODS-Eurofer, the evolution of such nanograins was never detected for any of the implemented production parameters and therefore their appearance is a key difference between both alloy types.

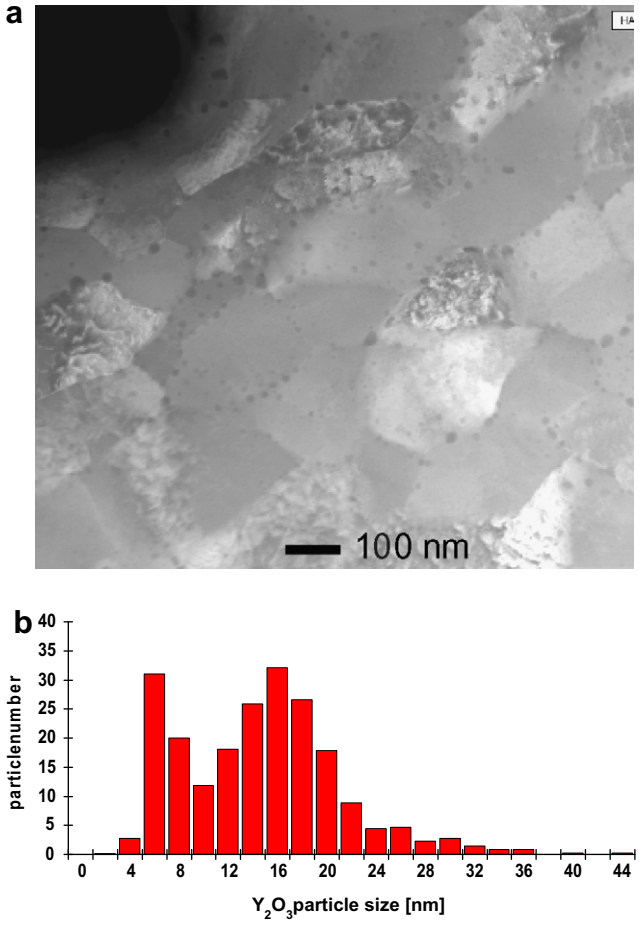

Fig. 3. (a) HAADF image of RAF ODS-alloy (13Cr–1W–0.3Y_2O_3) and (b) average Y_2O_3 particle size distribution (size step 2 nm).

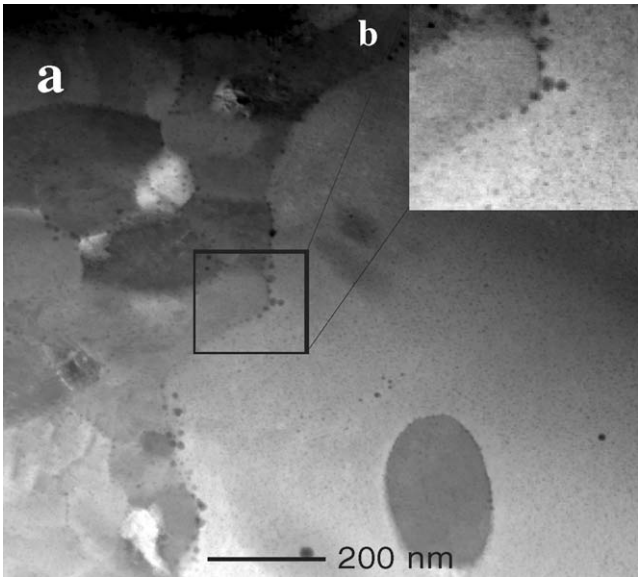

Fig. 4. (a) HAADF image of nanometer/micrometer grain boundary of RAF ODS-alloy (13Cr–1W–0.3Y_2O_3) and (b) enlarged grain boundary with ultrafine ODS-particles.

Bright field imaging (BF) and a high annular dark field detector (HAADF) were used to compare the ODS-particle characteristics of both materials. ODS-particles were recognized as dark contrasted dots using both imaging modes. Fig. 2(a) shows such a BF image for ODS-Eurofer: the spatial particle distribution is relatively homogeneous. Fig. 2(b) displays the overall particle size distribution, which was determined through analyses of several images. A wide range of particle sizes is created, as clearly shown in Fig. 2(a). A particle size peak is located at around 12 nm, but even particles up to 40 nm can be found.

When comparing the ODS-particle morphology in the RAF-ODS-steel to this, the bimodality of grain sizes must be considered. Fig. 3(a) shows firstly a nanometer grain region and Fig. 3(b) depicts the corresponding particle size distribution. Similarly ODS-particles are homogeneously distributed and mostly located at the nanometer grain boundaries. The particle sizes are more differentiated compared to ODS-Eurofer, two peaks around 6 nm and 16 nm were detected within the nanometer grain areas, but equally other sizes up to 44 nm exist. A smaller amount of particles >20 nm was recognized for both ODS-steels.

Furthermore the micrometer grain areas of the RAF-ODS-steel have also been investigated in detail. Another interesting phenomenon appeared, as Fig. 4(a) shows: on the right side of the HAADF image, a nanometer grain field, as described before, is located and bordered by a micrometer grain field on the left side. The borderline between the two fields is enlarged in Fig. 4(b). In the micrometer grain area an extremely high density of homogeneously

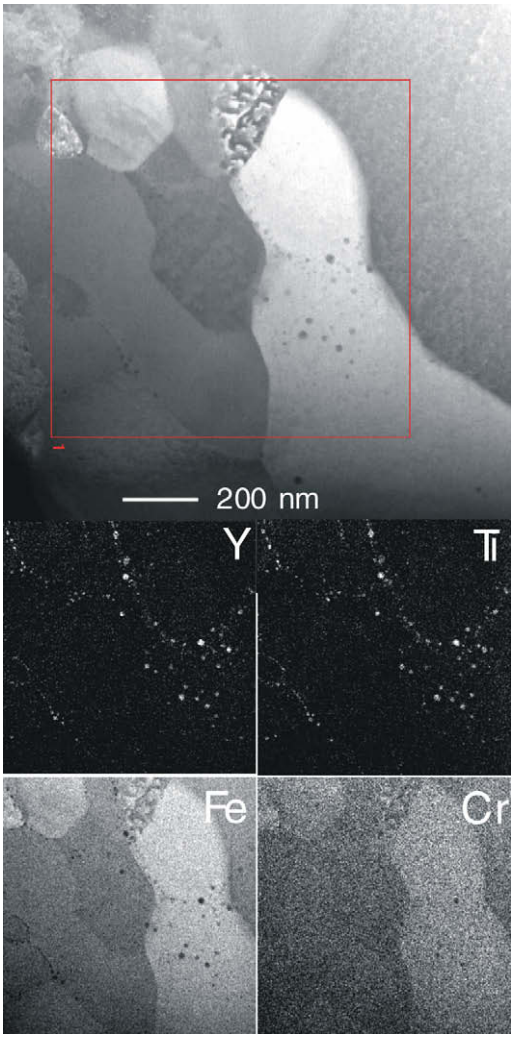

Fig. 5. HAADF image of the RAF-ODS-steel with elemental mappings of characteristic elements for the indicated area 1.

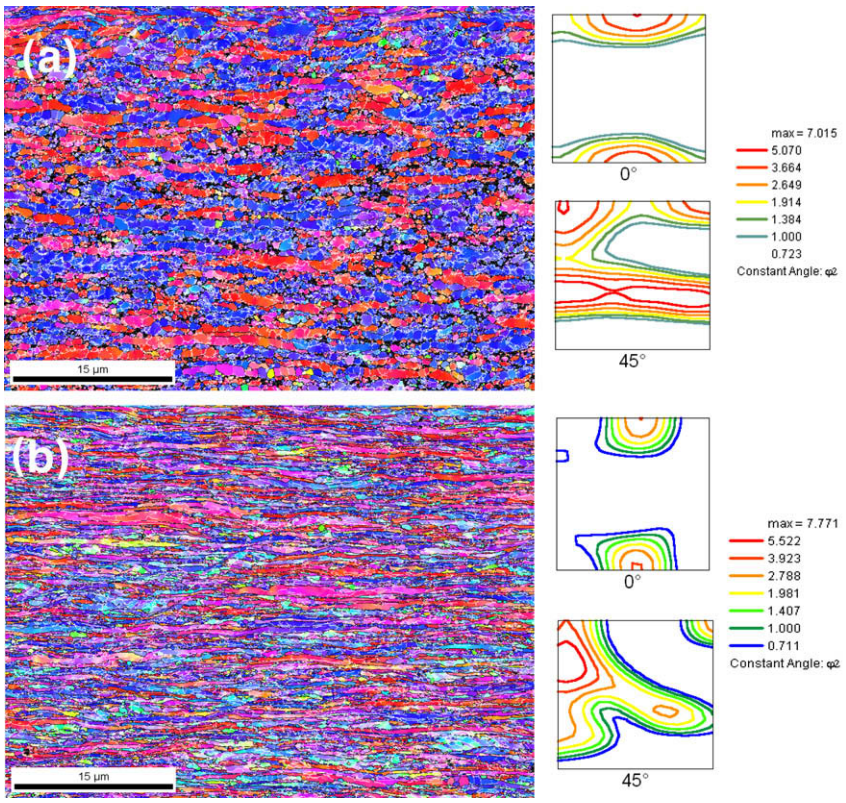

Fig. 6. (a and b) High-resolution EBSD maps of RAFM ODS-Eurofer steel after 50% and 80% reductions followed by annealing at 1073 K for 1 h and corresponding ODF sections ($\varphi_2 = 0$ and 45°).

distributed ultrafine ODS-particles (3–4 nm) was detected. Consequently, it has to be stated that there is also bimodality in ODS-particle sizes within the RAF-ODS-steel. The appearance of such ultrafine ODS-particles in ODS-Eurofer cannot be fully excluded, because indications for their existence were recognized. Investigations in this area are still ongoing. Generally due to detection problems it is very difficult to create reliable overall particle size statistics including these ultrafine particles with the method depicted in Figs. 2(b) and 3(b).

Additionally an elemental mapping with characteristic elements was carried through for another nanograin region in the RAF-ODS-steel, shown in Fig. 5. In elemental mappings bright contrasts stay for a high element concentration. The bright spots in the Y and Ti signal together with missing Fe and Cr contents on these positions is congruent to the spots in the HAADF image. It can be seen, that particles are not only located at the grain boundaries, but also within the nanometer grains themselves. Due to these results, the ODS-particle formation is clearly proven.

3.2. EBSD analyses and orientation maps

In order to obtain a more detailed understanding of the properties of these ODS-steels, texture and mesotexture analyses are of great importance too. That is why characteristic EBSD analyses were conducted firstly for the RAFM ODS-Eurofer alloy. Similar investigations for the RAF-ODS-steel are in progress.

Recrystallization during service life has to be avoided in this class of steels when exposed to the high temperatures during operation. The presence of a stable dispersion of fine particles is very effective to prevent recrystallization in metallic materials [7].

Cold rolling was successfully performed up to 80% in the RAFM steel. The Vickers microhardness numbers of this steel after 50% and 80% cold rolling are, respectively, 391 ± 5 and 425 ± 5. Annealing at 1073 K for 1 h did not cause a significant softening of this material. The respective Vickers microhardness numbers following annealing are, respectively, 382 ± 4 and 396 ± 7. The amount of softening is low, about 4% and 7%, respectively, indicating that the volume fraction of recrystallized grains is also very low.

The high-resolution EBSD scans revealed important details of the annealed structure of the ODS-Eurofer steel. Fig. 6 shows two scans performed in samples deformed to 50% (Fig. 6(a)) and 80% (Fig. 6(b)) reductions, respectively, and annealed at 1073 K for 1 h. Elongated grains along the rolling direction are found

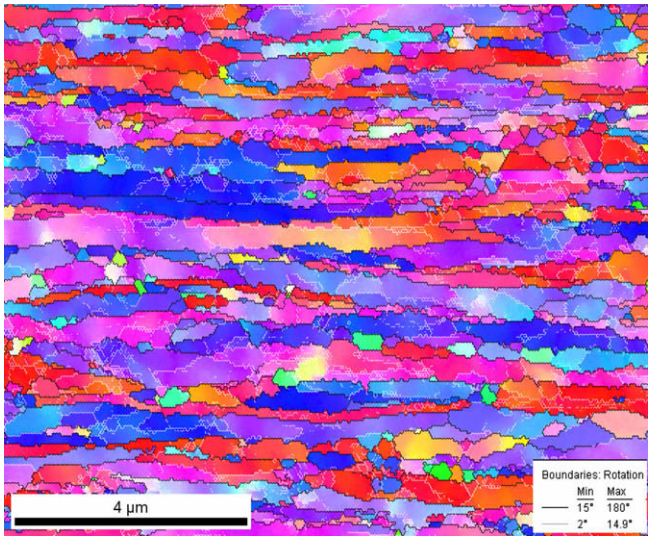

Fig. 7. Orientation map showing low and high angle boundaries in the RAFM ODS-Eurofer steel deformed to 80% and annealed at 1073 K for 1 h.

throughout the microstructure. They mostly belong to the α- and γ-fibers. Coarser features are noticed in the less deformed specimen. The corresponding ODF sections (φ_2 = 0 and 45°) corresponding to the microtexture provided by the orientation maps are also shown in Fig. 6. The microtexture components found in this steels are typical of low-carbon steels (rotated cube at φ_2 = 0° and α- and γ-fibers at φ_2 = 45°). The γ-fiber, for instance, is more pronounced in the less deformed specimen; however, direct comparisons must take into account local effects in texture.

A closer inspection of the orientation maps reveals the presence of small crystallites (smaller than 500 nm) bounded by high angle boundaries. They correspond to very fine equiaxed recrystallized grains contrasting with the elongated morphology of the surrounding recovered grains and are mostly found at the prior grain boundaries. The greatest advantage of using high-resolution EBSD is the possibility of to determine the volume fraction of high angle boundaries in large areas. The mesotexture of the sample deformed to 80% and annealed at 1073 K for 1 h is shown in Fig. 7. Due to intrinsic limitations of the technique, we have included only boundaries with misorientations larger than 2°. Only TEM is able to resolve lower misorientations accurately.

4. Summary

Through application of a definite production process according to the powder metallurgical route two different types of ODS-steels, the RAFM ODS-Eurofer and a RAF-ODS-alloy have been manufactured with the involvement of industrial partners. The microstructures of both alloys have been analysed and were compared. While ODS-Eurofer displays a more homogeneous grain size distribution, a bimodal grain size distribution, depending on the production parameters [2], was observed in the ferritic ODS-alloy. The reason for that needs further investigation, especially the influence of alternate HIP temperatures on the microstructure. Possibly this bimodality could lead to inhomogeneous deformation mechanisms in the ferritic ODS-steel compared to ODS-Eurofer, resulting in poorer mechanical properties. This needs to be proven.

ODS-particles were equally retrieved and confirmed. Generally the ODS-particle morphology was not much different in between both materials. Larger particles up to 40 nm and indications of ultrafine particles are existent. In case of the ferritic ODS-steel the bimodal grain size distribution was taken into account for the ODS-particle analyses. But the possible particle influence (e.g. grain boundary pinning) in formation of the bimodal grain size distribution in only one alloy type must be taken into account and analysed further.

The preliminary results of high-resolution EBSD are very encouraging. The microstructure of the deformed specimens is slightly softened by recovery. However, they also confirm the presence of tiny equiaxed recrystallized grains in the most deformed sample at 1073 K for 1 h. TEM is essential to resolve the boundaries with misorientations below 2° and the nature of particle-boundary interaction during recovery/recrystallization reactions in this particle-containing material.

References

[1] R. Lindau, M. Klimenkov, A. Möslang, M. Rieth, B. Schedler, J. Schröder, A. Schwaiger, Proceedings of the 16th International Plansee Seminar, Reutte, Austria, 2005, p. 545.
[2] Ch.Ch. Eiselt, M. Klimenkov, R. Lindau, A. Möslang, published at ICFRM13, (Nice, 10–14.12.2007), submitted to J. Nucl. Mater.
[3] S. Ukai, M. Fujiwara, J. Nucl. Mater. 307–311 (2002) 749.
[4] P. Miao, G.R. Odette, T. Yamato, M. Alinger, D. Hoelzer, D. Gragg, J. Nucl. Mater. 367–370 (2007) 208.
[5] H. Kishimoto, M.J. Alinger, G.R. Odette, T. Yamamoto, J. Nucl. Mater. 329–333 (2004) 369.
[6] Z. Oksiuta, N. Baluc, J. Nucl. Mater. 374 (2008) 178.
[7] F.J. Humphreys, M. Hatherly, Recrystallization and Related Annealing Phenomena, Pergamon, Oxford, 1996.